Advanced Steel Construction – Vol. 21 No. 3 (2025) 265–276
DOI:10.18057/IJASC.2025.21.3.8

SEISMIC PERFORMANCE OF SQUARE CORE TUBE SQUARE STEEL TUBE COLUMN FULLY BOLTED CONNECTION JOINTS

Hai-Ling Bao [1], Pei-Bao Xu [2], Kai Li [2] and Zi-Qing Yuan [3, *]

[1] *Anhui Technical College of Water Resources and Hydroelectric Power, Hefei, Anhui 231603,China*
[2] *Department of Civil Engineering Anhui Jianzhu University, Hefei, Anhui 230601,China*
[3] *School of Civil Engineering, Hefei University of Technology, Hefei, Anhui 230009, China*
** (Corresponding author: E-mail: yuanziqing@mail.hfut.edu.cn)*

ABSTRACT

Traditional steel structures often use full penetration welding for square steel tube column-to-column connections, which is labor-intensive and challenging to quality control. Prefabricated connections using high-strength bolts reduce welding but require drilling holes in the columns, potentially compromising stiffness and load-bearing capacity. To mitigate these issues, this paper introduces a novel fully bolted connection joint for square core tube square steel tube columns. This joint comprises outer extension end plates for both the column and the core tube, which are secured together using high-strength bolts. No holes needed in the steel tube wall, which ensures the stiffness and load-bearing capacity of the connection area, and allows for fully prefabrication. To reveal the working mechanism of proposed joint, finite element models were established using ABAQUS software. The entire stress process of the joint under low-cycle reciprocating loads was analyzed. The analysis examined how parameters like core tube strength, thickness, square steel tube column strength, axial compression ratio, and bolt pre-tension affected key mechanical performance indicators such as plastic deformation, failure modes, hysteresis, and energy dissipation. The results indicate that the core tube can increase the stiffness at the connection location, causing the plastic development region to be far from the connection area, achieving the seismic design goal of 'strong joints, weak members'. Meanwhile, the joint's hysteresis curves exhibit fullness without evident pinching, with ductility coefficients ranging from 2.66 to 3.79, inter-story displacement angles fall ranging from 1/98 to 1/71, which meets the GB50011-2010 specifications. Optimal design suggests a square steel tube to core tube strength ratio of 1.5-1.78, core tube to column strength ratio of 0.22-0.66, and axial compression ratio of 0.3-0.5. The core tube to column thickness ratio and bolt type should be selected based on structural needs. The research confirms the joint's feasibility and provides design guidance.

ARTICLE HISTORY

Received: 28 September 2024
Revised: 6 January 2025
Accepted: 8 January 2025

KEYWORDS

Prefabrication;
Square steel tube column connection joint;
High-strength bolt connection;
Seismic performance;
Finite element analysis

1. Introduction

In prefabricated steel structures, the mechanical behavior of column base connections is vital for structural integrity. These joints bear vertical and lateral loads. Traditional connection methods usually involve equal-strength welding and high-strength bolts[1-3]. Equal strength welding, with its strong integrity, still risks stress concentration and pre-existing defects at the welds[4-7]. The adoption of high-strength bolts in connections enhances the structural safety margin and reduces on-site installation duration, facilitating full assembly on-site[8,9].

In the current landscape of prefabricated steel structure design, column-to-column connection joints are primarily classified into flange connection joints [10-14] and sleeve-type connection joints [15-18]. Wang et al [10, 11] studied steel tube flange connections through experiment and finite element methods. A practical design method for circular steel tube flange joints was developed using the virtual work principle and T-shaped end plate model. Couchaux et al[12] conducted experimental investigations on 6 flange column connection joints, resulting in the development of an analytical model for the compression deformation of flange connection joints. This model incorporates considerations of the flange's bending-torsional behavior and the opening-closing actions of the joints. Huang et al[13] experimentally and numerically studied two types of specimens: one for upper column base joints and another for lower column top joints. The study's outcomes revealed that both specimens exhibited bending failure in the concrete column sections. Furthermore, the high-strength bolt flange connection specimen demonstrated hysteresis performance comparable to that of the steel tube full-length specimen, categorizing it as an "equal strength connection." Zhang et al[14] thoroughly investigated beam-column to column flange joints in prefabricated steel structures, proposing design parameter adjustments for effective damage control. The results demonstrate that the proposed design optimizations can safeguard structures during extreme scenarios such as earthquakes, mitigate component failure, and facilitate rapid functional recovery. Flange-type column connection joints are crucial in prefabricated steel structures, and their appropriate design and construction are vital for ensuring structural safety and stability. In conclusion, flange connection joints exhibit a range of desirable attributes, including broad applicability, convenient installation and maintenance, and high levels of reliability. Nonetheless, further comprehensive research is required to enhance the understanding of the systematic testing and theoretical aspects of both flexible and rigid flange connection joints.

In the context of sleeve-type connection joints, Qiu et al[15] have investigated a flange splicing joint designed for the connection of tubular fiber reinforced polymer (FRP) components. Their research findings suggest that an insertion depth of 100mm for square steel tubes into FRP tubes is optimal, guaranteeing adequate bonding strength and load-bearing capacity. Chu et al[16] have introduced a novel double-flange sleeve-type column-column-beam connection joint. Combining experiments and simulations, their research examines how factors like axial compression ratio, sleeve wall thickness, and height affect joint seismic performance. Furthermore, simplified formulae were proposed to determine the yield and ultimate load-bearing capacities of this innovative connection joint. Wu et al[17] created a fully bolted joint for planar modular steel structures. The joint features square steel tube columns with built-in sleeves, connected to H-shaped beams using angle steels and plates. The study shows that the joint displays semi-rigid behavior, and using high-strength bolts for vertical joints and thicker angle steels improves its seismic resistance. Xia Junwu et al[18] conducted comprehensive experimental investigations on a novel spliced outer sleeve joint. The findings highlight the exceptional rotational capability of this joint, with the beam-column angle surpassing 0.06 radians, signifying a high level of flexibility. In conclusion, the advantages of sleeve connection joints are their straightforward construction and cost-effectiveness, which enhance the construction efficiency of light steel structures, achieve superior fastening outcomes, and facilitate full bolt connections in closed cross-sections. Dai et al. [19] developed an innovative insertion-type self-locking connection joint and conducted thorough experimental research on its performance. Drawing from their experimental findings, a simplified mechanical model was proposed and design recommendations for the joint were offered, aiding in its effective implementation. Lancy et al. [20] have introduced a novel modular interlocking connection joint designed for modular steel building structures. This joint integrates bolts with interlocking components, thereby enhancing construction efficiency and significantly improving the joint's resistance to slippage. Sendanayake et al[21] introduced two types of modular joints with extra steel plates and elastic layers, aiming at transferring the potential failure points of the structure from the columns to the modules, facilitating elastic deformation of the interconnection joints.

Building on current research, this paper introduces a novel design for a fully bolted connection joint in square core tube square steel tube columns, which facilitates full assembly while ensuring structural stiffness and load-bearing capacity. This design represents an improvement over previous flange and sleeve connection methods, as it maintains structural integrity and load-bearing capacity while prioritizing full prefabrication and enabling rapid post-earthquake repairs. The study utilizes ABAQUS software to develop 14 finite

element models, investigating how key parameters such as core tube strength, thickness, square steel tube strength, bolt type, and axial compression ratio influence the seismic performance of the proposed joint. The findings are anticipated to provide new insights for the advancement of prefabricated steel structures.

2. Joint design and working principle

2.1. Joint design

The prefabricated joint is consist of upper and lower square steel tubes, a square core tube equipped with external end plates, and high-strength bolts. An external end plate connects the upper and lower columns by high-strength bolts. A core tube within the column strengthens the joint, improving its bending and shear resistance. The construction of this connection joint is illustrated in Fig. 1.

2.2. Stress analysis and force transmission path

Analyzing the stress distribution at a 4% inter-story displacement reveals the vertical stress S33 distribution of the component, depicted in Fig. 2, and the horizontal stress S11 distribution, illustrated in Fig. 3. The vertical stress S33 distribution within the square core tube joint indicates that the bending moment is effectively converted into a tension-compression couple, which is transmitted through the column walls on either side. The couple passes through the bolt holes to the square core tube, then via its flange to the lower section, and along the core tube's wall to the column foot.

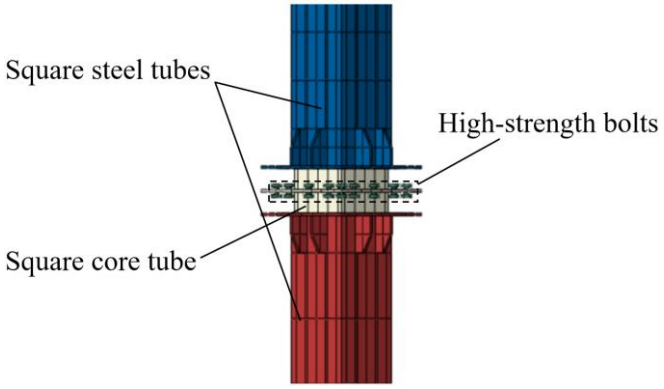

Fig. 1 Schematic of the square core tube square steel tube column fully bolted connection joint

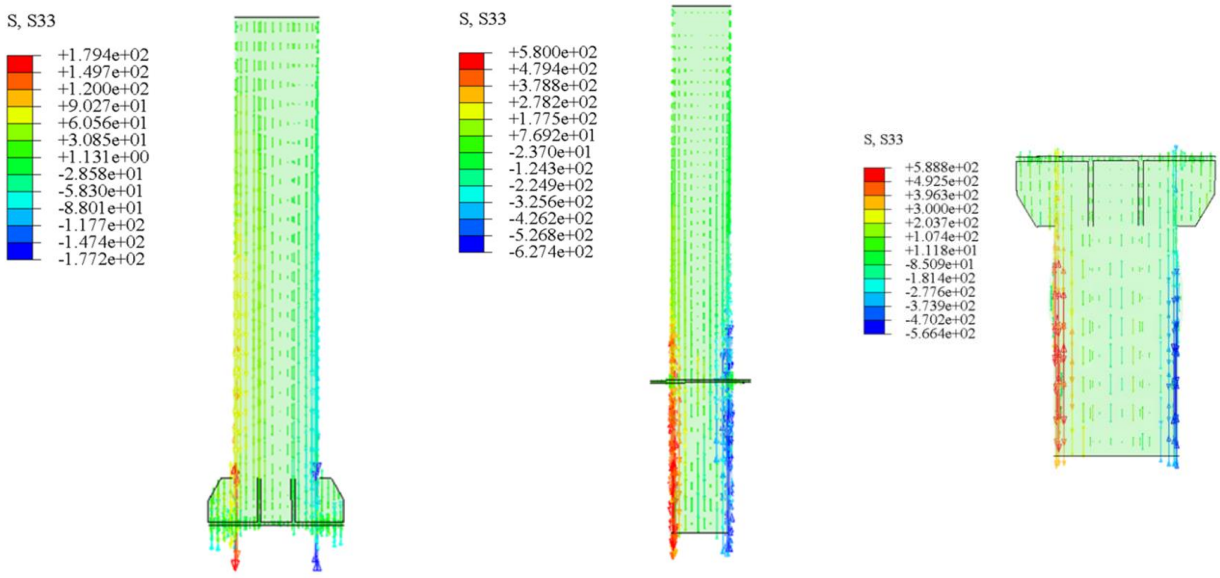

(a)S33 stress distribution of upper steel tube column (b)S33 Stress distribution of core (c)S33 stress distribution of lower steel tube column

Fig. 2 S33 Stress distribution of column

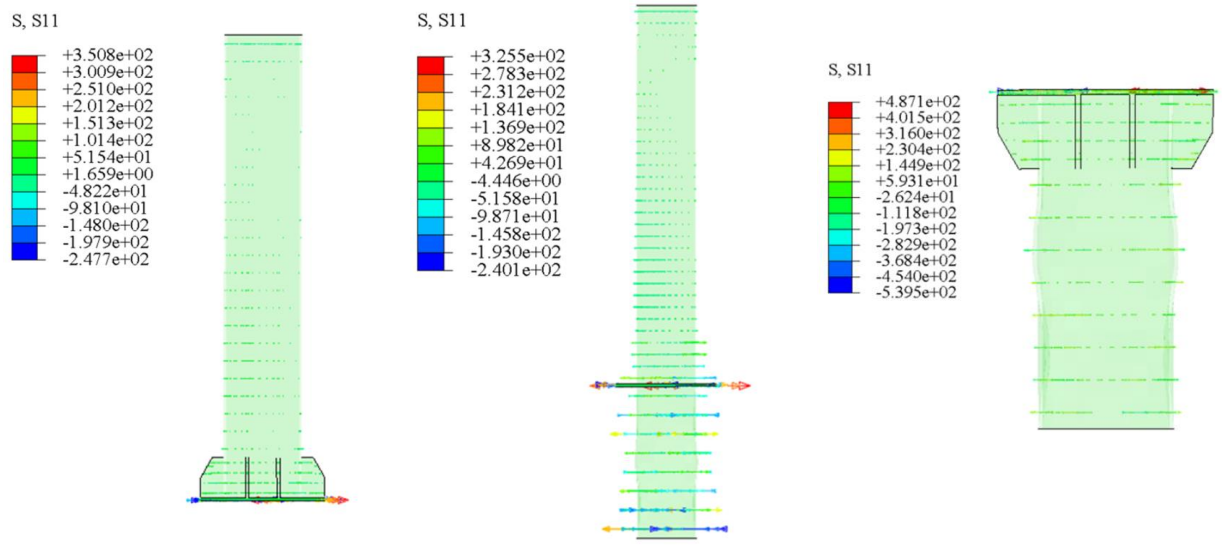

(a)S11 stress distribution of upper steel tube column (b)S11 Stress distribution of core (c)S11 stress distribution of lower steel tube column

Fig. 3 S11 Stress distribution of column

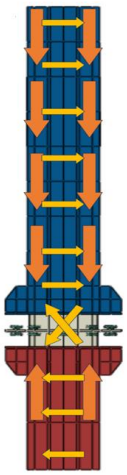

Fig. 4 Force transmission path

As shown in Fig. 3, the stress distribution at node S11 indicates that the horizontal shear force at the column top is transmitted through the upper steel tube to the bolt holes. This force is subsequently transmitted through the bolts to the square core tube wall, then to the lower steel tube wall, and continues its transmission along the column wall to the column base. Fig. 4 illustrates the force transmission path of the joint.

3. Model establishment

3.1. Model geometry

A total of 12 joint models have been designed across 4 groups, with comprehensive parameter details provided in Table 1. The first-floor column of the prototype structure, made from a 500mm×500mm×16mm square steel tube, stands at a height of 4200mm. Fig. 5 shows the detailed dimensions of the column base joint.

Additionally, the core tube inside the joint serves to increase the stiffness of the column's joint area. The core tube's dimensions must be chosen based on the balance between its bending strength and that of the outer steel tube to prevent joint interface damage.

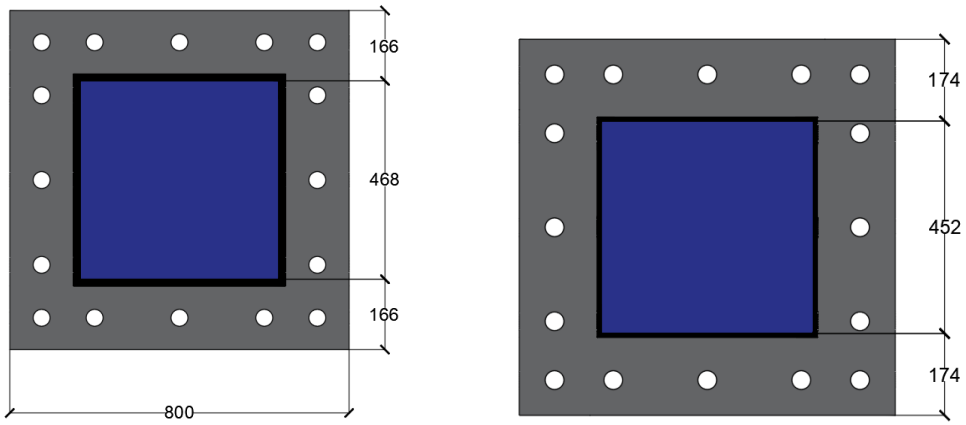

(a)Details of column dimensions (b)Details of core tube dimensions

Fig. 5 Section sizes of core tube components(mm)

Table 1
Details of joints parameters (mm)

Model No.	Steel tube size(mm)	Core tube size(mm)	Steel tube grade	Core tube frade	Axial compression ratio	Bolt type
JD-1	500×500×16	468×468×10	Q355	Q235	0.3	M24
JD-2	500×500×16	468×468×10	Q420	Q235	0.3	M24
JD-3	500×500×16	468×468×10	Q460	Q235	0.3	M24
JD-4	500×500×16	468×468×10	Q355	A6061	0.3	M24
JD-5	500×500×16	468×468×10	Q355	LY160	0.3	M24
JD-6	500×500×16	468×468×10	Q355	Q355	0.3	M24
JD-7	500×500×16	468×468×10	Q355	LY160	0.2	M24
JD-8	500×500×16	468×468×10	Q355	LY160	0.4	M24
JD-9	500×500×16	468×468×10	Q355	LY160	0.5	M24
JD-10	500×500×16	468×468×10	Q355	LY160	0.6	M24
JD-11	500×500×16	468×468×12	Q355	LY160	0.3	M24
JD-12	500×500×16	468×468×14	Q355	LY160	0.3	M24
JD-13	500×500×16	468×468×10	Q355	Q235	0.3	M27
JD-14	500×500×16	468×468×10	Q355	Q235	0.3	M30

The design choices for the strength ratios, axial compression, and thickness ratios of the column and core tube, as well as the selection of bolt sizes, are the result of a meticulous engineering process aimed at optimizing the joint's structural performance, safety, and cost-effectiveness. The strength ratio of the column to the core tube, ranging from 1 to 4.4, is carefully selected to ensure that the column can withstand the expected loads without excessive material use, while also providing a sufficient safety margin against failure. This range allows for a graduated response to varying load conditions, preventing over-strength columns that could be unnecessarily costly and heavy. The core tube's strength ratio to the column, varying between 0.22-1, is set to ensure that the core tube contributes adequately to the overall stiffness and load-bearing capacity of the joint, without being so strong as to be wasteful or so weak as to become a potential point of failure. The axial compression ratio, which spans from 0.2 to 0.6, is chosen to maintain a balance between the column's ability to resist

compressive forces without experiencing buckling and its capacity to support the joint's weight and environmental loads. This range provides a buffer against both the risks of structural collapse and the potential for excessive deformation that could affect the joint's functionality. The column to core tube thickness ratio, established between 0.625 and 0.875, is a critical parameter that influences the joint's performance and the overall efficiency of the structure. This ratio ensures that the core tube is sufficiently thick to provide the necessary strength and stiffness while avoiding the use of excessive material, which could increase the structure's weight and cost. The selected range is a balance between structural requirements and economic considerations. Finally, the use of bolts sizes M24 to M30 for the connections between the column and core tube is a design choice that takes into account the mechanical properties of the fasteners, such as tensile strength and shear capacity. These bolt sizes are commonly used in structural applications and offer a range of options that can be tailored to the specific load requirements at each joint, ensuring that the connections are neither under-strength, which could compromise safety, nor over-strength, which could lead to unnecessary costs and complications during construction. The selection of bolt sizes is also influenced by the ease of installation, the availability of materials, and the potential for future maintenance or modifications to the joint.

3.2. Element type and meshing

The finite element model incorporates C3D8R solid elements for all components, with considerations for integration and hourglass effect[22]. To account for the complex forces present at the joint, the mesh in the flange area is densified to ensure the accuracy of the analysis data. Smaller mesh sizes are employed for high-strength bolts and core tubes during mesh generation, with the mesh size for high-strength bolts set at 10mm and that for core tubes at 20mm. The model components are shown in Fig. 6.

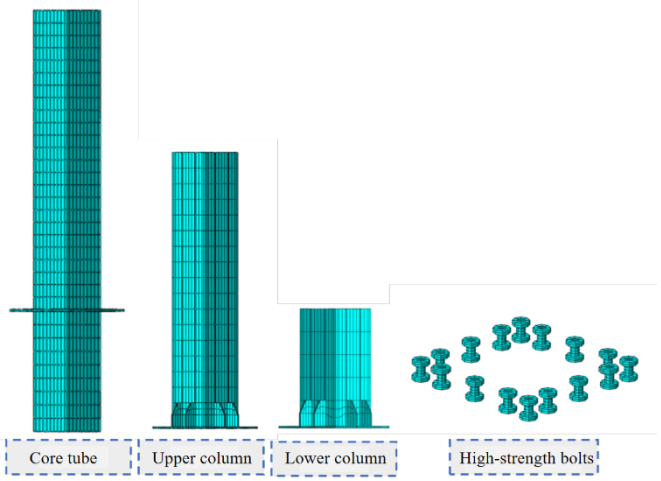

Fig. 6 Meshing

3.3. Constitutive models

The steel material's elastic modulus is taken as Es=2.06×105 N/mm^2, poison ratio is 0.3. The constitutive model of high-strength bolt adopts multi-linear isotropic strengthening model[23]. The nominal value of 10.9 grade high strength bolt is adopted as $f_y = 980\ MPa$、$f_u = 1100 MPa$。The constitutive model for ordinary strength steel and low yield strength steel utilize the framework proposed in literature [24], which incorporates plateau and hardening segments. An initial 100kN pre-tightening force is applied to the bolt, then increased to 240kN for model convergence. Subsequently, the bolt rod dimensions are maintained at their current lengths throughout the analysis steps, ensuring that the bolt pre-tightening force adjusts dynamically with the model's displacement response.

3.4. Boundary conditions and loading approach

Fig. 7 illustrates the specific configurations for contact and boundary conditions of the model, the interaction between the bolt, nut, and the steel tube and core tube is characterized by "hard contact". Additionally, the tangential interaction among these components adopted coulomb friction model[2], with a specified coefficient of friction of 0.45. To ensure a fully rigid connection at the column foot, fixed boundary conditions are implemented at this location. The high-strength bolt connections are restrained to prevent lateral instability of the components. A coupled reference point is positioned at the column top, through which both horizontal and vertical loads are applied, with a compressive load of 0.3 times the column's axial compression ratio applied at the top.

Following AISC seismic specifications, a displacement-controlled variable amplitude loading method is used for horizontal loading. Each loading level encompasses two cycles, with the levels progressively increasing to 0.00375, 0.005, 0.0075, 0.01, 0.02, 0.03, and 0.04 rad. The loading protocol is outlined in Fig. 8 for clarity.

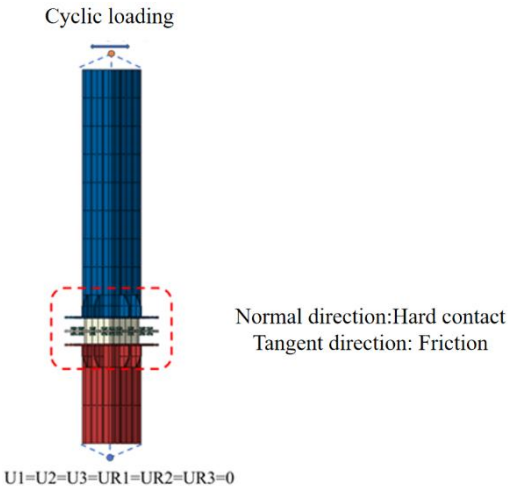

Fig. 7 Boundary conditions

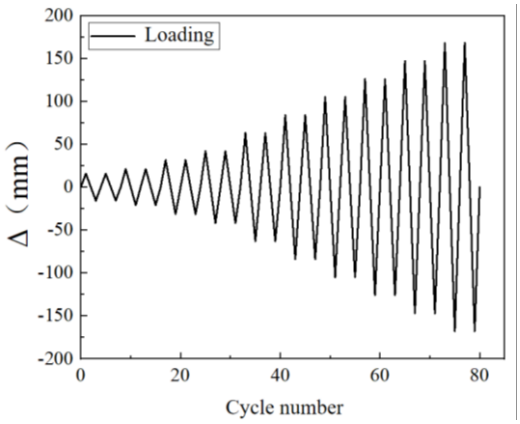

Fig. 8 Loading system

4. Model validation

4.1. Failure mode

To verify the finite element model's accuracy, a comparative simulation analysis was conducted using the test case from literature [25]. The test joint configuration in the referenced literature closely mirrors that of the joints in the present study, with the element selection and mesh division in the validation model aligning with those reported above. Fig. 9 compares the failure modes in the finite element simulation with the experimental results from the literature.

The joint underwent cyclic loading as described, reaching a 7% inter-story displacement. Fig. 9 shows a significant bulge in the eastern steel tube wall at the column base, which is in substantial agreement with the column wall bulging observed in the experimental setup.

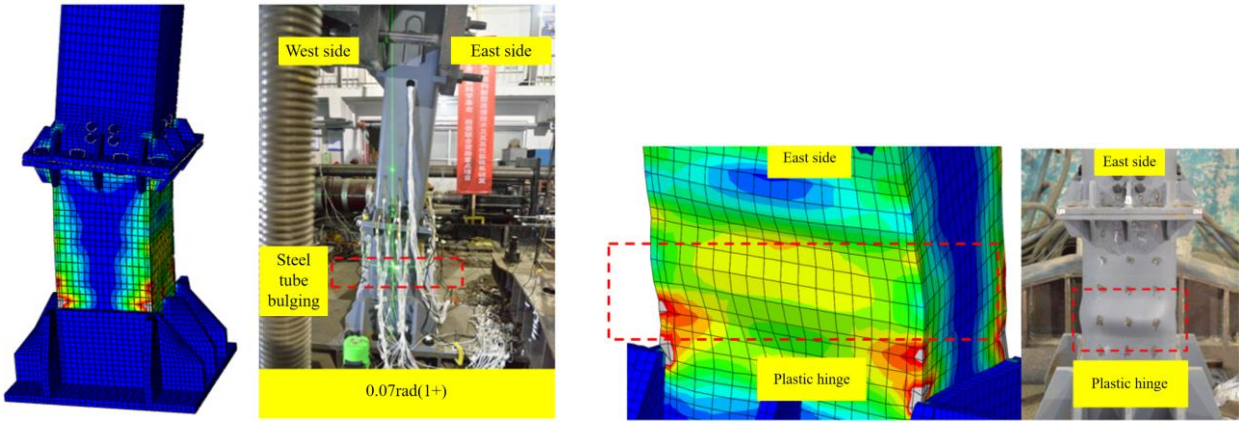

Fig. 9 Comparison of failure mode

4.2. Verification of hysteresis curves and skeleton curves

Fig. 10 provides a comparative analysis of the hysteresis and skeleton curves of experiment and simulation results. Fig. 10 illustrates that the hysteresis and skeleton curves from the finite element analysis closely align with the experimental results, particularly in the aspect of initial stiffness. The finite element analysis reveals that the positive and negative peak bearing capacities from the model are lower than the experimental results by approximately 7.1% and 9.8%, respectively, with both differences falling within a 10% margin. The results suggest that the finite element modeling approach employed is effective in simulating the mechanical properties of proposed joint under cyclic load conditions.

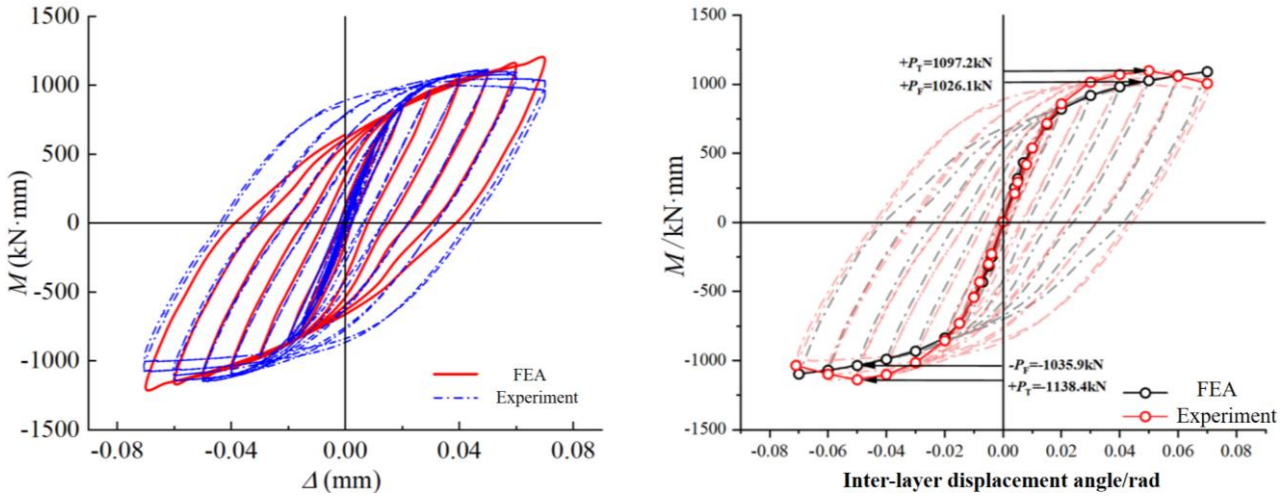

(a) Hysteresis curves

(b) Skeleton curves

Fig. 10 Comparison of calculation results

5. Mechanical performance of core tube

5.1. Failure mode

Fig. 11 displays the equivalent plastic stress contours for various parameters at a 4% inter-story displacement angle, revealing significant bulging in the steel tube column walls at the column foot. This observation indicates the potential for local deformation and failure under seismic loads, highlighting the need for robust design and construction practices to prevent such issues.

The relationship between the grade upgrade of the square steel tube and the corresponding increase in plastic stress levels at the column foot, as shown in Fig. 11(a), suggests that material selection is crucial. Higher-grade materials can withstand greater stresses but may also be more prone to brittle failure. Therefore, a balance must be struck between material strength and ductility to ensure the joint's performance under seismic events.

Fig. 11(b) demonstrates that with the increase in core tube strength, the plastic stress level at the column foot decreases. This finding implies that strengthening the core tube can enhance the joint's overall seismic performance. It suggests that optimizing the core tube's design, rather than simply increasing the strength of the square steel tube, may be a more effective strategy for improving joint performance.

The axial compression ratio's significant effect on the mechanical properties of the joints, as highlighted in Fig. 11(c), indicates that proper consideration of this parameter is essential. A higher axial compression ratio increases the vertical load on the column, which can lead to higher stress concentrations and potential failure modes. The axial compression ratio should be carefully evaluated in the designing process to ensure the joint can safely withstand expected loads.

Fig. 11(d) emphasizes the importance of the core tube thickness and bolt model in enhancing the joint's performance. Increasing the core tube thickness improves its contribution to the square steel tube column, while upgrading the bolt model increases the bolt pre-tension force, improving the stress level at the column base. However, the modest influence of the bolt model upgrade on seismic performance suggests that other factors, such as material selection and joint geometry, may have a more significant impact.

In summary, the strength ratio of the square steel tube column in relation to the core tube, as well as the thickness ratio of the core tube to the square steel tube, significantly affect the plastic stress levels at the column foot in column-to-column connection joints. The understanding of these relationships is crucial for designing joints that can withstand seismic loads and prevent failure modes such as local deformation, brittle failure, and stress concentrations. Considerations of these factors and ensure proper reinforcement and detailing to enhance the joint's overall performance and safety are needed in the practical designing.

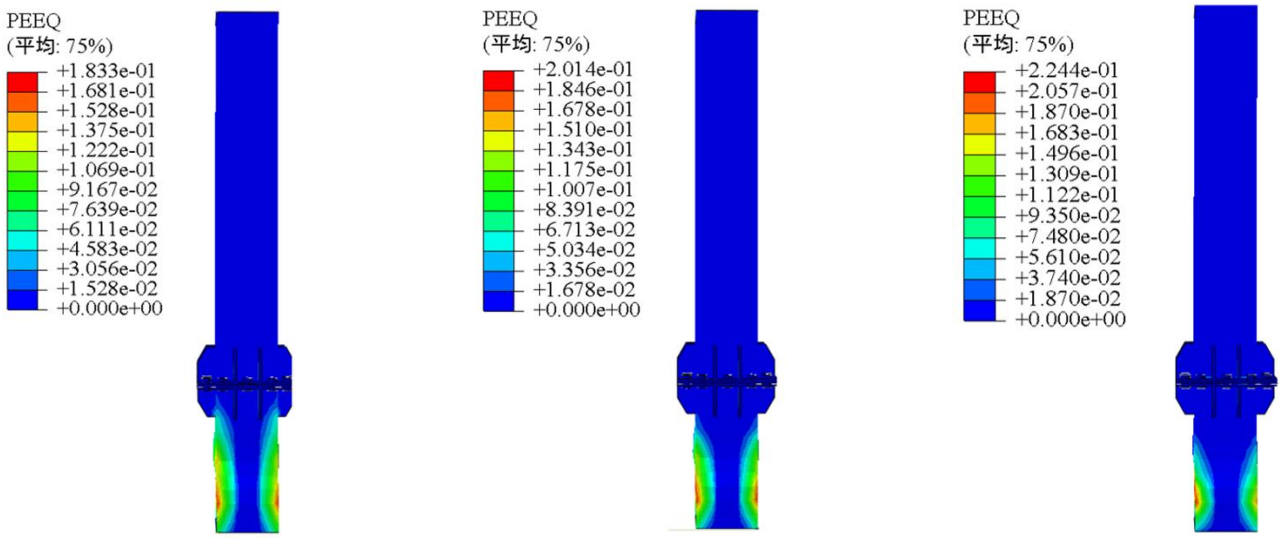

(a)Comparison of JD-1, JD-2, JD-3

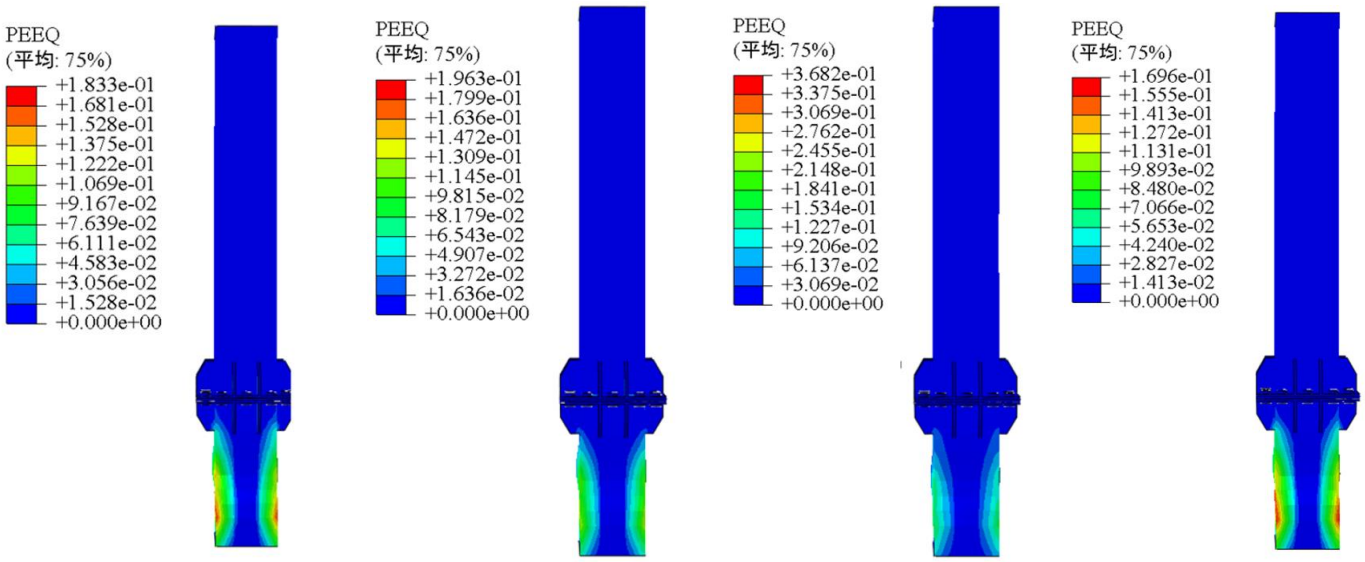

(b)Comparison of JD-1, JD-4, JD-5,JD-6

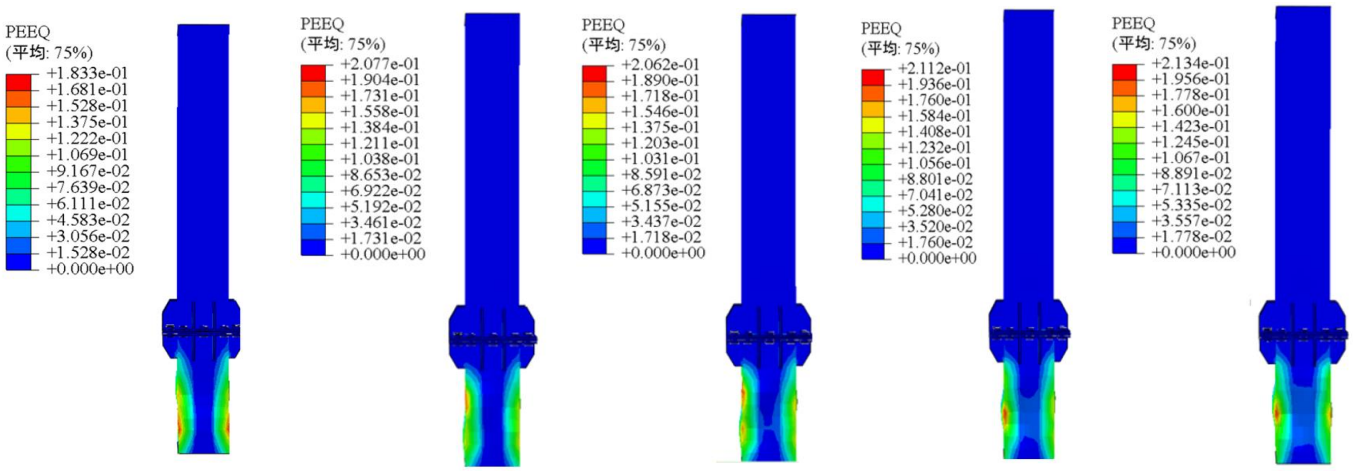

(c)Comparison of JD-1, JD-7, JD-8,JD-9, JD-10

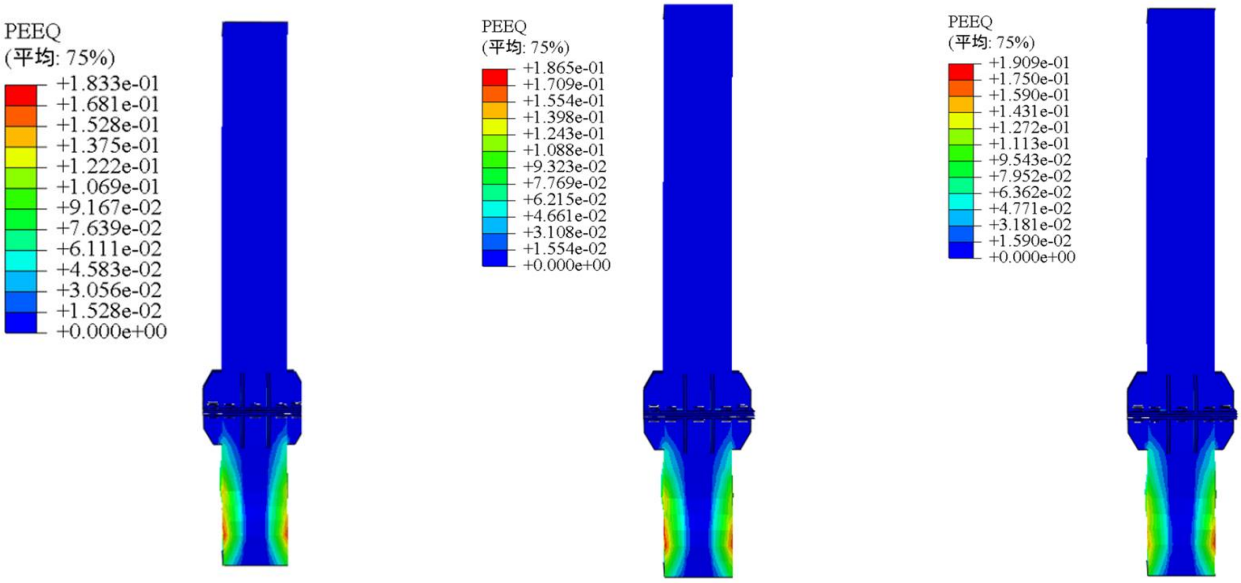

(d)Comparison of JD-1, JD-11, JD-12

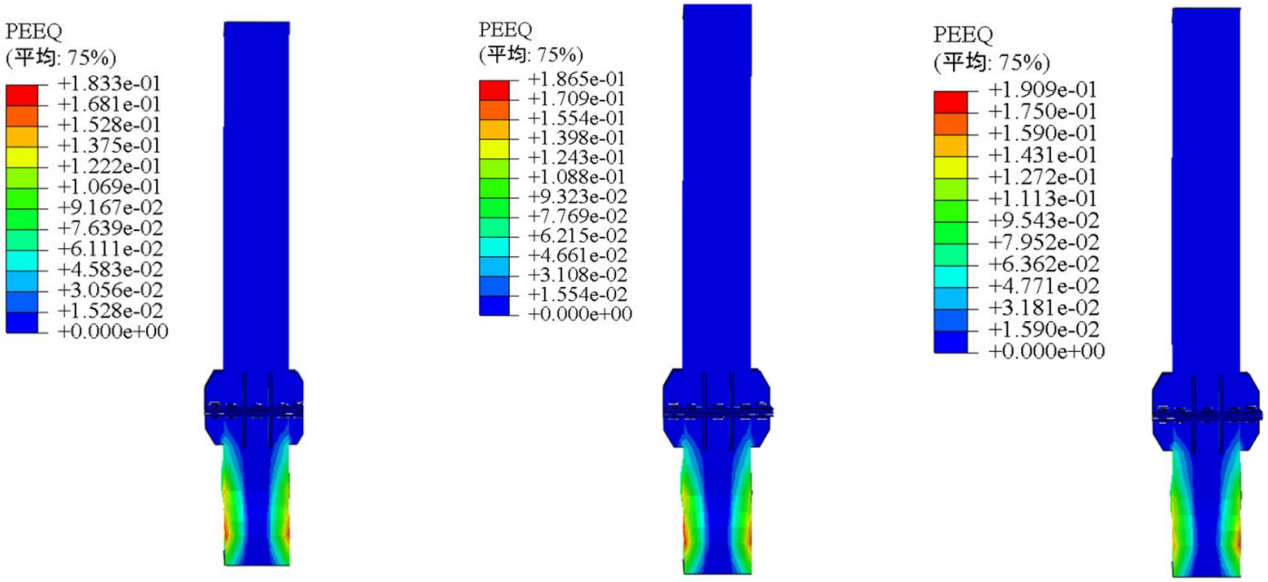

(e)Comparison of JD-1, JD-13, JD-14

Fig. 11 Comparison of equivalent plasticity

5.2. Stress analysis

Fig. 12 presents the stress diagram obtained from the lower column's S1 path. It is observed that the column base undergoes yielding with stresses above 355 MPa. As the strength ratio of the square steel tube relative to the core tube increases, there is a corresponding increase in stress at the column base, with the impact remaining within a 10% range. As illustrated in Fig. 12(c), the stress at the column base increases continuously with the axial compression ratio, with the increment ranging from 11% to 24%. Furthermore, Figs. 12(d) and 12(e) demonstrate that under a 4% inter-story drift, the thickness ratio between the column and core tube and the bolt model exert a relatively small effect on the stress at the column foot, within a 5% limit.

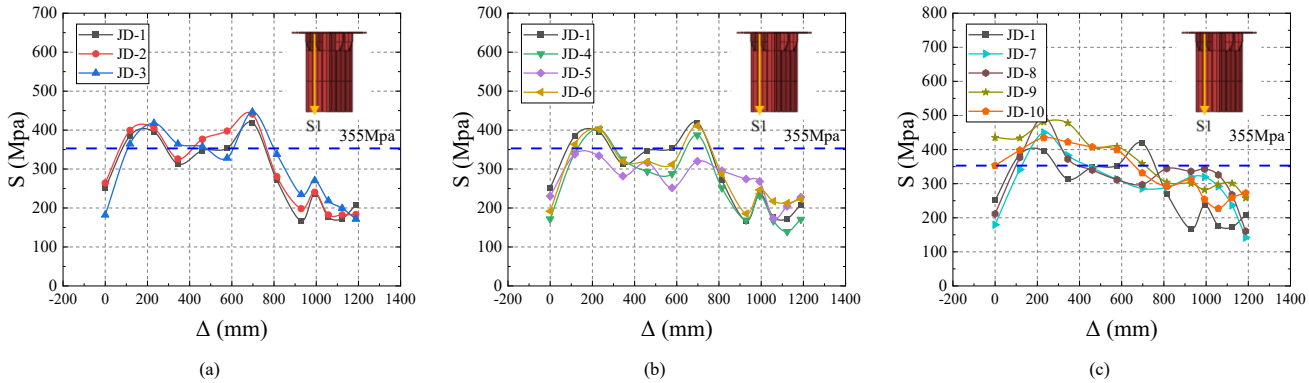

(a) (b) (c)

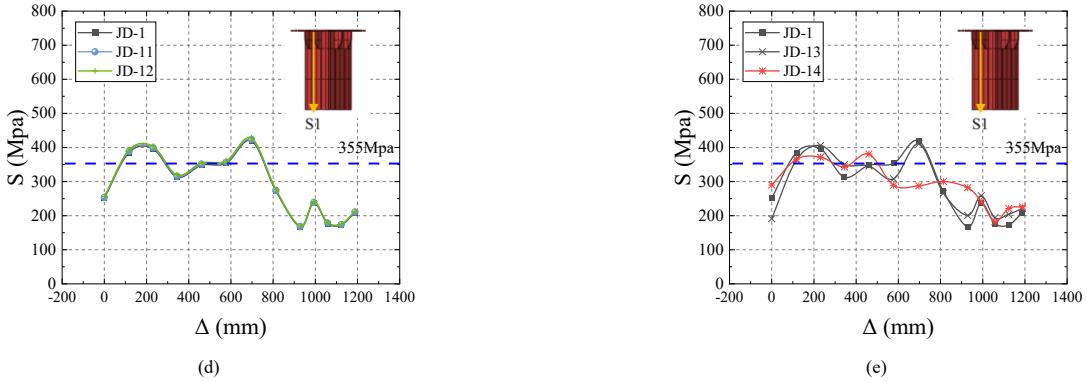

Fig. 12 Stress analysis

5.3. Hysteresis performance

Fig. 13 displays the hysteresis curves for models JD1-JD14. It is apparent from the figure that these curves are robust and exhibit no significant pinching phenomena, indicating that the connection joints possess a high capacity for energy dissipation. The strength ratio of the column to the core tube, as shown in Fig. 13(a), directly effects the bearing capacity and the completeness of the hysteresis curves. This suggests that strengthening this ratio effectively improve the hysteresis performance of the joints. In Fig. 13(b), the models' ultimate bearing capacity increases with the core tube-to-column strength ratio, highest when strengths match. Fig. 13(c) shows joint capacity reduction with axial compression ratio, 21% less at 0.6 than 0.3, recommending a ratio between 0.3 and 0.5. Figs. 13(d) and 13(e) suggest minimal influence of thickness ratio and bolt preload force on joint properties.

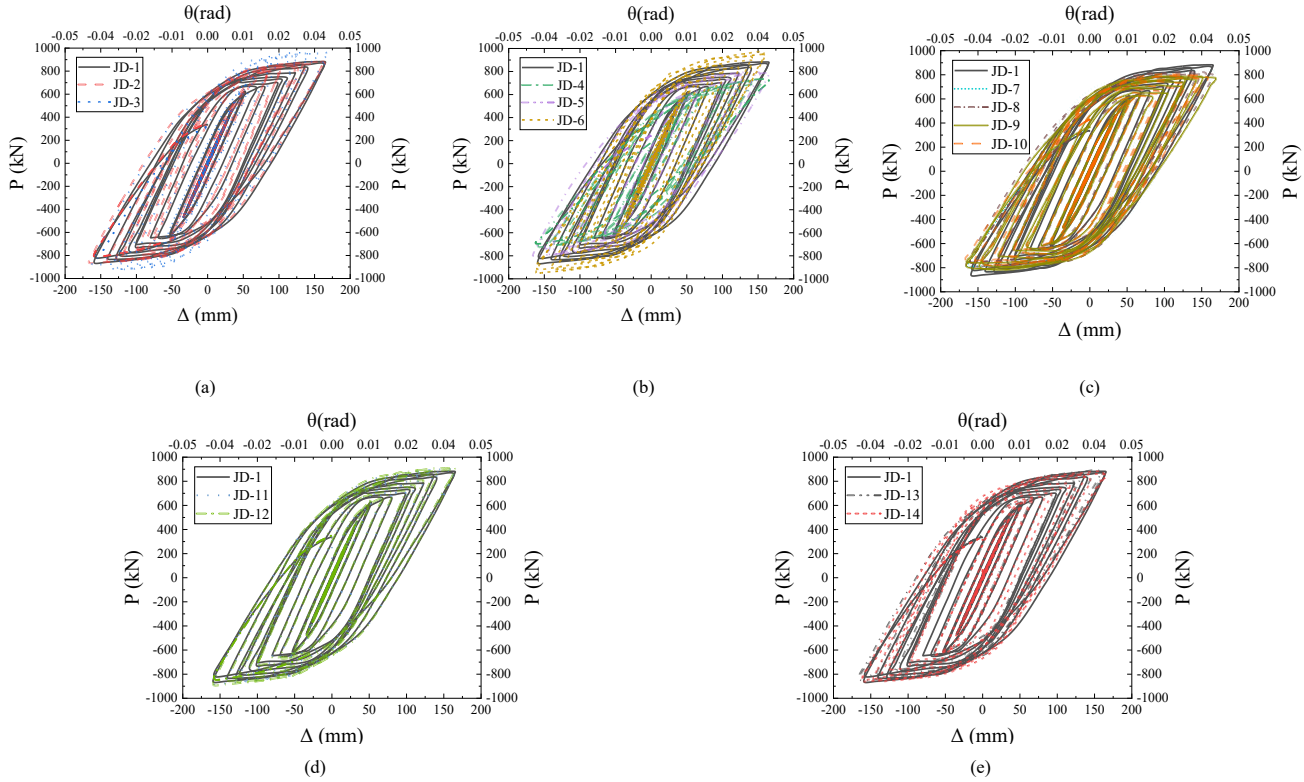

Fig. 13 Comparison of hysteresis curves

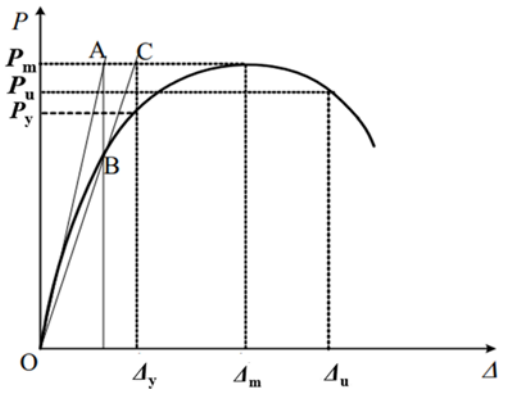

Fig. 14 Schematic of determining yield point by yield moment method

5.4. Skeleton curves

In accordance with the guidelines provided in the JGJ101-2015 code [26], it is essential to accurately determine the yield load, yield displacement, failure load, and failure displacement for the column-to-column connection joints. The yield load is ascertained through the application of the yield moment method. In Fig. 14, a tangent line, labeled OA, is drawn on the initial segment of the skeleton curve. Additionally, a horizontal line is constructed at the peak of the curve. The intersection of OA with the horizontal line occurs at point A. A perpendicular line is then drawn through point A, intersecting the skeleton curve at point B. By connecting points OB and extending this line to intersect the horizontal line at the peak, the x-coordinate at this intersection, point C, denotes the yield displacement(Δ_y), the y-coordinate of the skeleton curve indicates the yield load(P_y). The coordinates of the peak point denote the ultimate load(P_m) and ultimate displacement(Δ_m). The coordinate values corresponding to 0.85 times the P_m are designated as the failure load P_u and the failure displacement Δ_u. This facilitates the identification of the characteristic points on the $P-\Delta$

relationship curve.

Fig. 15 presents the skeleton curves for the various models studied. The initial stiffness remains stable despite variations in the column to core tube strength ratio, axial compression ratio, column thickness ratio, and bolt model. However, the strength ratio of the core tube to the column notably influences the initial stiffness of the specimens. A significant change in stiffness is observed at a 1% inter-story displacement angle, with stiffness decreasing progressively as the inter-story displacement angle increases. Following the peak load, there is a decreasing trend in the load as displacement continues to increase.

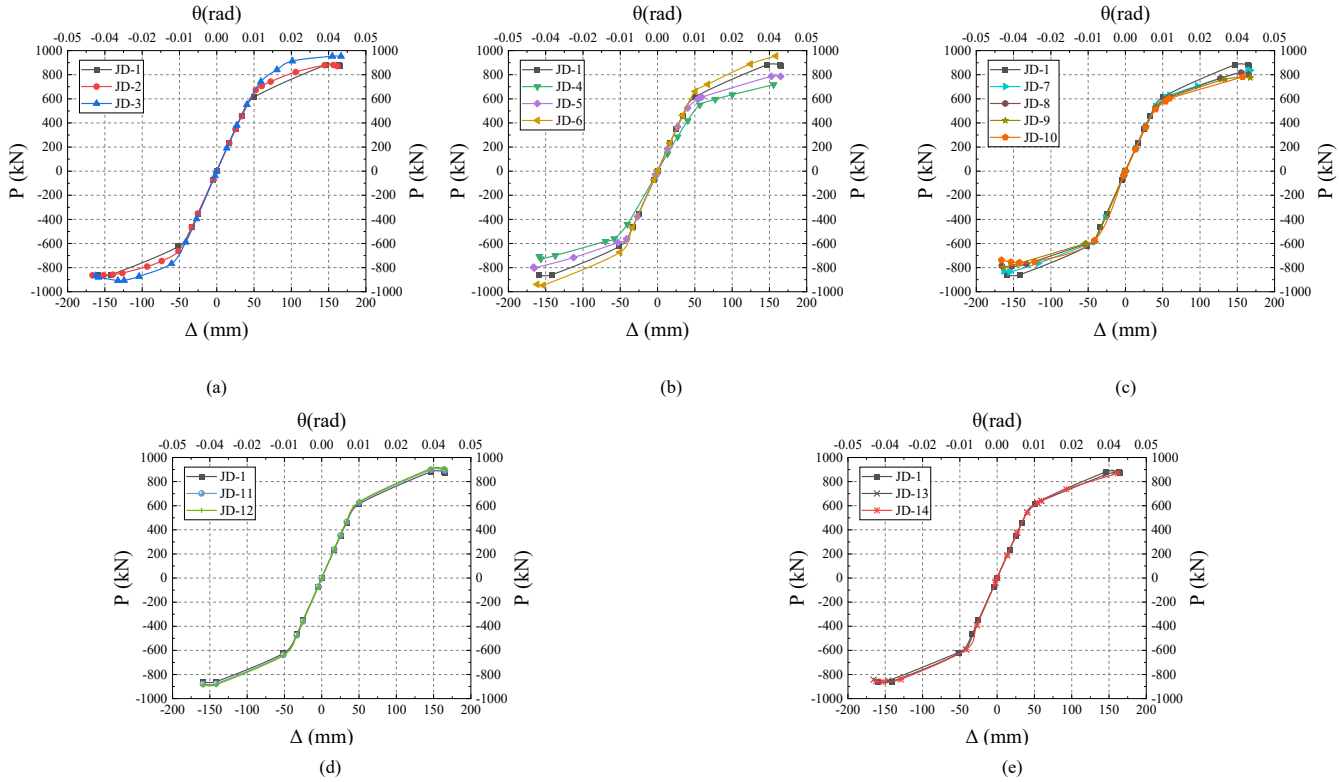

Fig. 15 Comparison of skeleton curves

5.4.1. Load capacity

A detailed comparison of the structural integrity of different models has been carried out, with a focus on parameters such as stiffness, ductility, and inter-story displacement angle. This analysis is based on the calculation results of key mechanical indicators from the skeleton curve, as detailed in Table 2. The data illustrates that as the ratio of column strength to core tube strength increases, there is a noted enhancement in the yield bearing capacity of the model by 6.71% and 9.05%, respectively. Conversely, the ultimate bearing capacity experiences a decrease of 1.14% and 1.17%. This trend indicates that an escalation in the column to core tube strength ratio is inversely proportional to the model's overall bearing capacity. As the column to core tube strength ratio increases, the model exhibits varying degrees of change in yield bearing capacity, including a decrease of 2.58%, an increase of 2.32%, and a substantial increase of 27.87%. Conversely, the ultimate bearing capacity shows a significant reduction, with decreases of 24.48%, 17.19%, and 0.51%. As the axial compression ratio of the model increases, the yield bearing capacity progressively enhances by 10.92%, 8.85%, 5.17%, and 4.48%. Conversely, the ultimate bearing capacity undergoes a significant reduction, with decreases of 11.87%, 13.98%, 18.33%, and 21.95%. To ensure optimal structural integrity, maintaining the axial compression ratio within the range of 0.3 to 0.5 is recommended. In addition, as the thickness ratio of the core tube to the columns increases, the model's yield bearing capacity is notably enhanced, with increases of 2.34% and 19.96% observed. Furthermore, an increase in the bolt pretension force leads to improvements in yield bearing capacity by 15.51% and 16.42%.

The analysis reveals intricate trends in the seismic performance of the joint, with the column to core tube strength ratio showing a significant influence on the yield bearing capacity, which enhances as the ratio increases. However, this comes at the expense of a decrease in the ultimate bearing capacity, indicating an inverse relationship. The axial compression ratio also plays a critical role, with an increase leading to enhanced yield bearing capacity but a notable reduction in ultimate bearing capacity, suggesting a balance is necessary for optimal structural integrity. Furthermore, the thickness ratio of the core tube to the columns emerges as a more influential factor than the bolt pretension force, with increases in this ratio resulting in substantial improvements in yield bearing capacity. Although the bolt pretension force has a moderate impact, it still contributes to enhancements in yield bearing capacity. The findings underscore the importance of carefully considering these design parameters to achieve the desired balance between yield and ultimate bearing capacities, ensuring the safety and integrity of the structure under seismic conditions.

Table 2
Key mechanical indicators

Model No.	Loading direction	Yield capacity Py (kN)	Ultimate capacity Pu (kN)	Yield displacement Δ_y (mm)	Displacement ductility coefficient μ	Yield displacement angle θ_y
JD-1	+	607.8	950.2	53.99	2.92	1/78
JD-2	+	648.6	939.4	55.68	2.87	1/75
JD-3	+	662.8	933.7	59.27	2.66	1/71
JD-4	+	592.1	717.6	51.92	3.04	1/81
JD-5	+	621.9	786.9	54.31	2.91	1/77
JD-6	+	777.2	955.0	56.71	2.79	1/74
JD-7	+	674.2	837.4	50.42	3.13	1/83
JD-8	+	661.6	817.4	48.99	3.23	1/86
JD-9	+	638.6	776.0	43.06	3.67	1/98
JD-10	+	635.0	741.6	41.74	3.79	1/80
JD-11	+	622.0	900.2	54.12	2.92	1/78
JD-12	+	729.1	909.0	54.28	2.91	1/77
JD-13	+	702.1	875.8	53.85	2.93	1/78
JD-14	+	707.6	869.5	52.70	3.00	1/80

5.4.2. Ductility and inter-story displacement angle

The ductility of a structure is commonly assessed using two key parameters: the displacement ductility coefficient and the rotation ductility coefficient. The

displacement ductility coefficient μ can be calculated with Eq. (1), where Δ_u and Δ_y are displacements of the column ends when structure fails:

$$\mu = \Delta_u / \Delta_y \quad (1)$$

Utilizing the data for yield and failure displacements from Fig. 15, the coefficient is computed in accordance with Eq. (1), with the comprehensive results presented in Table 2. In compliance with GB50011-2010 code, the permissible elastic displacement angle for steel structures is 1/250. The results presented in Table 2 indicates that the positive yield displacement angles for the integrated square core tube joints fall within the range of 1/71 to 1/98, adhering to the code's requirements for elastic inter-story displacement angles.

The data presented in Table 2 indicates that the ductility coefficients for the models with various parameters span from 2.66 to 3.79. Notably, the strength ratio of the columns to the core tube has a significant influence on the model's ductility, with a range of variation from 2.66 to 2.92. It is recommended that the strength ratio of the columns to the core tube be maintained within the range of 1.5 to 1.78. The continuous increase in the core tube's strength leads to a decrease in the model's ductility and deformation capacity. Consequently, it is suggested that the strength ratio of the core tube to the columns be no greater than 0.66. The axial compression ratio's increase is observed to enhance the model's ductility coefficient, while factors such as the thickness ratio of the core tube to the columns and the bolt pretension force type exert a relatively minor impact on the mechanical properties of the joints.

5.5. Energy dissipation capacity

The column base joint, when subjected to seismic forces, must exhibit a high capacity for energy dissipation, primarily through the plastic deformation of its components. This research employs the cumulative energy dissipation of hysteresis loops to conduct a quantitative analysis of the joint, as depicted in Fig. 16 and detailed in Eq. (2):

$$E = \frac{S_{(ABC+CDA)}}{S_{(OBE+ODF)}} \quad (2)$$

In which:

$S_{(ABC+CDA)}$ - area encompassed by the hysteresis loop at each load level, corresponding to the energy dissipation value at the joint.

$S_{(OBE+ODF)}$ -the area encompassed by the triangles OBE and ODF during one loading cycle.

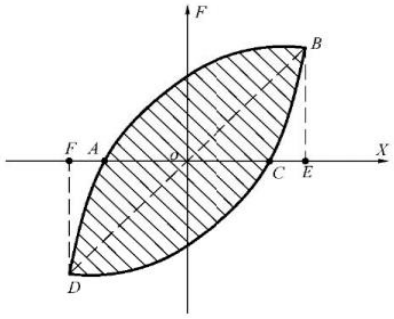

Fig. 16 Energy dissipation coefficient calculation diagram

Fig. 17 depicts the cumulative energy dissipation for the various models examined. It is evident that as the strength ratio of the columns to the core tube increases, there is a corresponding decrease in the model's cumulative energy dissipation. Compared to the JD-1 model, the cumulative energy dissipation for JD-2 and JD-3 is reduced by 4.2% and 6.8%, respectively. Contrarily, the analysis reveals that an increase in the strength ratio between the core tube and the column results in a significant enhancement of the joint's cumulative energy dissipation, with increases of 21.6%, 3.1%, and 2.2% observed relative to JD-1. This emphasizes the critical role of the core tube in energy dissipation within column-to-column connections and underscores the importance of the core tube's strength as a key parameter affecting the seismic resilience of proposed joints. Therefore, it is recommended to maintain the strength ratio of the core tube to the columns no less than 0.22. The analysis further reveals that the energy consumption ratio of the models initially increases and then decreases with the rising axial compression ratio. Consequently, it is advisable to maintain the axial compression ratio within the range of 0.3 to 0.5 for optimal performance. Additionally, the analysis indicates that the thickness ratio of the core tube to the columns has a negligible effect on the cumulative energy dissipation, with variations within a 3% range. Hence, this ratio can be determined based on specific structural design requirements. Furthermore, the models exhibit a decrease in cumulative energy dissipation during early loading stages as bolt strength increases. However, at a displacement angle of 4%, the cumulative energy dissipation among all models remains consistent, suggesting that while the bolt type significantly influences the initial energy dissipation, its effect on the model's behavior during the plastic-elastic phase is relatively minor.

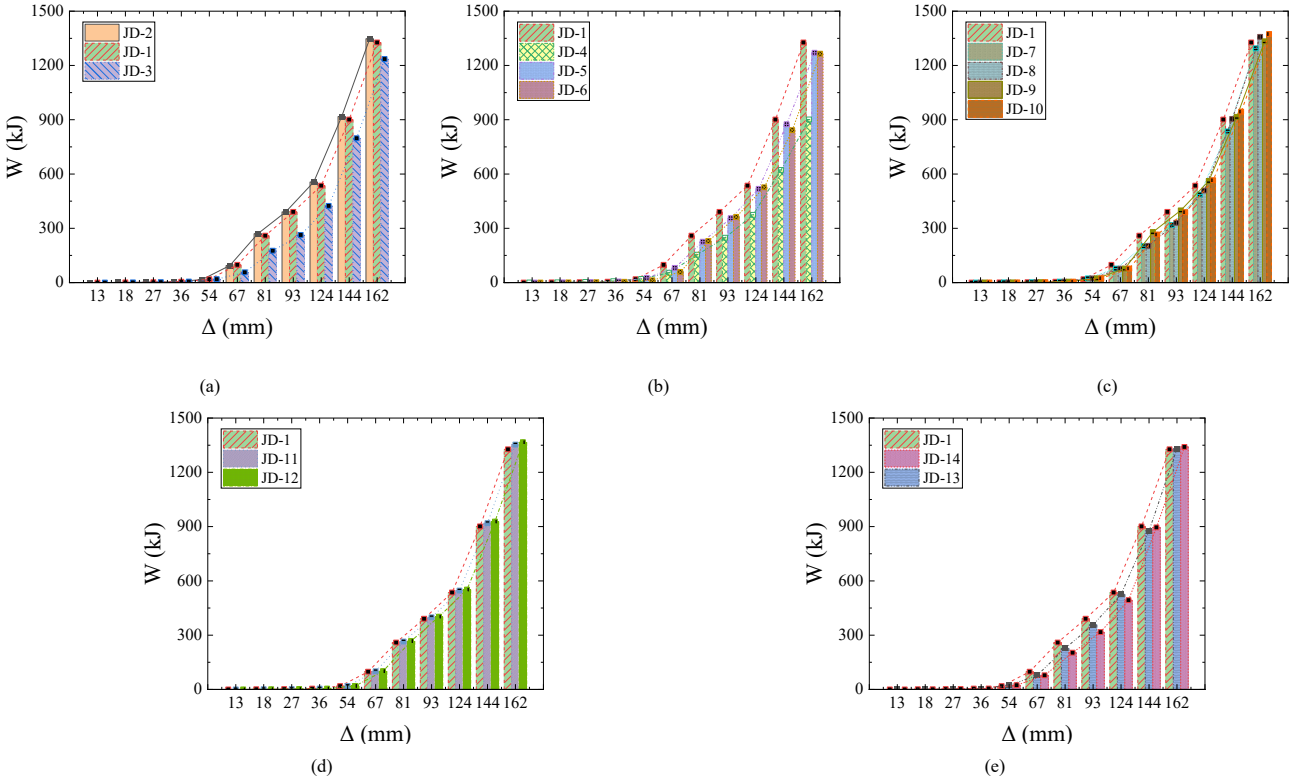

Fig. 17 Cumulative energy dissipation

5.6. Stiffness degradation

Upon the occurrence of damage within a structure or component, the $P-\Delta$ curve transitions from linear growth to a pattern of diminishing bearing capacity increments. Concurrently, the structural or component stiffness exhibits signs of degradation. The reduction in stiffness serves as a reflection of the cumulative damage progression within a structure, prompting the utilization of the stiffness degradation curve in this study to assess the seismic performance of column-to-column joints. The present work employs the secant stiffnessK_i, as recommended by the standard, to quantify the stiffness degradation of the joints with an integrated square core tube. This secant stiffness is defined as the slope of the line joining the peak load points under the same level of cyclic loading, with the calculation formula detailed in Eq. (3).

$$K_i = \frac{|+F_i| + |-F_i|}{|+\Delta_i| + |-\Delta_i|} \tag{3}$$

In which：

F_i-The peak load during the ith cycle of loading

Δ_i-The displacement value associated with the peak load during the ith cycle of loading

K_i-The secant stiffness for the ith cycle

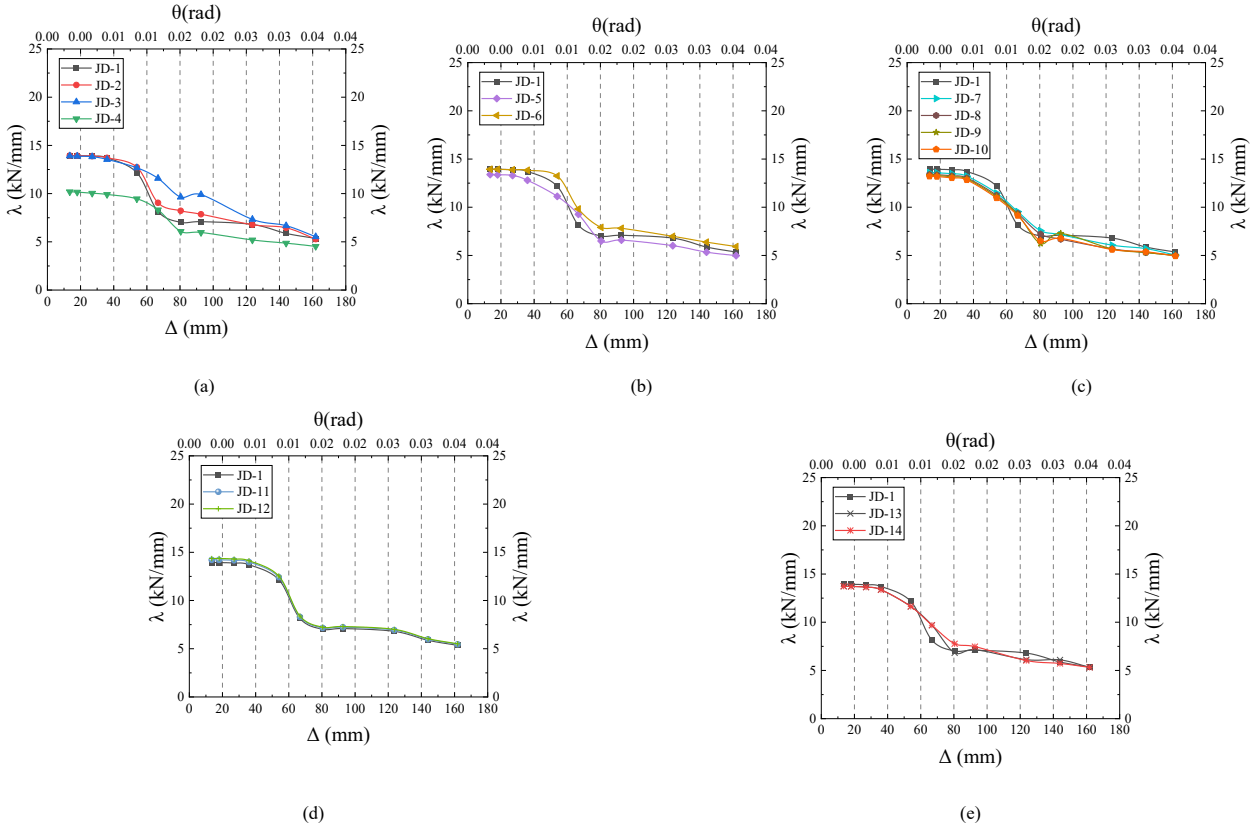

Fig. 18 Stiffness degradation comparison

Fig. 18 illustrates the stiffness degradation of each joint. It is obvious that prior to the 1% displacement angle, the stiffness of the models remains largely unchanged, indicating no significant degradation. However, beyond this threshold, a notable decline in stiffness is observed, with a reduction of 27% to 43%. The main factors influencing stiffness degradation include the strength ratio between the core tube and the column, the axial compression ratio, and the bolt pre-tension force. Conversely, the thickness ratio of the core tube to the columns has a lesser effect.

6. Conclusions

The study introduces a square core tube square steel tube column fully bolted connection joint, elaborating on the design principles and assembly process. Through ABAQUS software, finite element analysis models of the joint were created. The models facilitated the analysis of stress distribution within the joint under cyclic loading, elucidating the joint's failure mechanism and load transfer path. Subsequently, a parametric analysis was conducted to evaluate how key design parameters influence the joint's seismic performance.These parameters included the strength ratio of the column to the core tube, the axial compression ratio, the thickness ratio of the core tube to the column, and the bolt pre-tension force. The specific conclusions drawn from the study are as follows:

(1) A comprehensive finite element model of the joint was meticulously constructed. The accuracy of the finite element simulation was validated through a comparative analysis of the simulated hysteresis curves, skeleton curves, and failure modes against experimental data from pertinent studies.

(2) Detailed analysis was conducted to examine the plastic evolution and ultimate failure modes of the square core tube throughout the entire loading phase. The vertical and horizontal load transfer mechanisms of the column-to-column joint were identified. Throughout the loading process, the joint connections remained elastic, with plastic deformation confined to the bottoms of the core tube and the column, which adhered to the seismic design principle of "strong joints, weak members".

(3)The proposed joints have successfully realized the seismic design objective, conforming to the specified requirements for elastic and elastic-plastic inter-story displacement angles. The ductility coefficients across the models range from 2.66 to 3.79, with the elastic inter-story displacement angle varying between 1/98 and 1/71.

(4) The seismic performance of the joint is primarily influenced by three factors: the strength ratio of the column to the core tube, the strength ratio of the core tube to the column, and the axial compression ratio. Additionally, the bolt pre-tension force significantly affects the initial stiffness and energy dissipation capacity of the column, although the cumulative energy dissipation capacity remains consistent in the later stages. The recommended ranges for these parameters are as follows: the strength ratio of the column to the core tube should be between 1.5 and 1.78, the strength ratio of the core tube to the column should range from 0.22 to 0.66, and the axial compression ratio should be within the range of 0.3 to 0.5. Furthermore, the ratio between the core tube and the column thickness and the bolt type should both be selected based on the specific structural design requirements.

Funding

The research was funded by the Anhui Provincial Natural Science Foundation, Youth Project(2008085QA50).

References

[1] Wang Y Q, Liu, XY, Lin Y. Experimental study on fracture toughness of high-strength structural steel and its butt weld[J]. Advanced Steel Construction.2015,11(4):440-451.

[2] Jiao J F, Fan L X, Liu Y, et al. Investigating fatigue mechanisms and crack growth in 20mntib steel high-strength bolts: an experimental and simulation study[J]. Advanced Steel Construction.2023,19(4):329-340.

[3] Zhu Y P, Chen X Q, Zhong Y,et al.Seismic fragility analysis of steel frames with fully-bolted core tube joints[J]. Advanced Steel Construction.2024,20(3):208-221.

[4] Xue P, Gao M. Stress magnification effect of initial deformation on the notch stress field and fatigue strength of thin plate welded joints[J]. International Journal of Pressure Vessels and Piping, 2023(206): 253-262.

[5] Yan R Z, Zhang C L, Wang S, el al. Distribution of residual steel in the sphere-pipe connection welds of welded hollow spherical joints[J]. Advanced Steel Construction.2023,19(3):262-272.

[6] Wu C, Liu J L, Wang R H.A study on the dynamic response of welded hollow spherical joints under impact loading[J].Progress in Steel Building Structures,2021,23(11):82-93.(in Chinese)

[7] Feng J, Jin J, Xia j, et al. Experimental study on seismic performance of pec composite column-steel beam beam frame with welded T-stub strengthened connections[J]. Advanced Steel Construction.2021,17(3):264-272.

[8] Vucetic V, Kostic M, Karadzic D. Reliability assessment of connections with slip-critical bolts and fillet welds in combination[J]. Journal of Constructional Steel Research, 2019(159): 289-299.

[9] Sha L, Tu F, Kang C Y. Study on seismic performance of cantilever beam-column connection with Z-shaped full-bolted joint with double friction surfaces at the flange[J]. Progress in Steel Building Structures,1-8[2024-12-29].(in Chinese)

[10] Zhang T, Wang Y, Li H. Cyclic behavior of column-to-column connections in novel prefabricated H-shaped steel beam to CFST column joint[J]. Journal of Constructional Steel Research, 2021(178): 106489.

[11] Wang Y Q, Zong L, Shi Y J. Bending behavior and design model of bolted flange-plate connection[J]. Journal of Constructional Steel Research, 2013, 84: 1-16.

[12] Couchaux M, Hjiaj M, Ryan I, et al. Bolted circular flange connections under static bending moment and axial force[J]. Journal of Constructional Steel Research, 2019, 157: 314-336.

[13] Zhang S, He X, Liu X. Bending-shear performance of column-to-column bolted-flange connections in prefabricated multi-high-rise steel structures[J]. Journal of Constructional Steel Research, 2021(178): 106488.

[14] Bao Y, Uy B. Connection design in modular steel construction: A review[J]. Journal of Constructional Steel Research, 2019(154): 193-209.

[15] Qiu C, Ding C, He X, et al. Axial performance of steel splice connection for tubular FRP column members[J]. Composite Structures, 2018, 189: 498-509.

[16] Chu Y, Zhong Y, Luo P, et al. Experimental study on the seismic performance of the new fully-bolted beam-column joint[J]. Journal of Constructional Steel Research, 2022, 199: 107619.

[17] Wang H, Zhao X, Ma G. Experimental study on seismic performance of column-column-beam joint in panelised steel-modular structure[J]. Journal of Constructional Steel Research, 2022, 192: 107240.

[18] Wu X, Hu Q, Zhang Z, et al. Analysis of bolted connection for H-section beam and square steel tube column[J]. Journal of Constructional Steel Research, 2018(148): 277-286.

[19] Dai X M, Zong L, Ding Y, et al. Experimental study on seismic behavior of a novel plug-in self-lock joint for modular steel construction[J]. Engineering Structures, 2019, 181: 143-164.

[20] Lacey A W, Chen W, Hao H, et al. New interlocking inter-module connection for modular steel buildings: Experimental and numerical studies[J]. Engineering Structures, 2019, 198: 109465.

[21] Sendanayake S V, Thambiratnam D P, Perera N, et al. Seismic mitigation of steel modular building structures through innovative inter-modular connections[J]. Heliyon, 2019, 5(11): e02751.

[22] D'Aniello M, Cassiano D, Landolfo R. Simplified criteria for finite element modelling of European preloadable bolts[J]. Steel and Composite Structures, 2017, 24(6): 643-658.

[23] Liu X C, He X N, Wang H X, et al. Bending-shear performance of column-to-column bolted-flange connections in prefabricated multi-high-rise steel structures[J]. Journal of Constructional Steel Research, 2018, 145(JUN.): 28-48.

[24] Han LH. Concrete-filled steel tubular structures [M]. Beijing: Science Press, 2004: 477. (in Chinese)

[25] Zhang Yanxia, Li Hongwei, Huang Zhewen, et al. Finite element analysis of the seismic performance of self-tapping bolt-core sleeve flange column connection nodes in prefabricated steel structures [J]. Journal of Beijing University of Civil Engineering and Architecture, 2023, 39(02): 98-104. (in Chinese)

[26] Ministry of Housing and Urban-Rural Development of the People's Republic of China. Code for seismic test of buildings: JGJ/T101-2015 [M]. Beijing: China Architecture & Building Press, 2015. (in Chinese)